J. Fluid Mech. (2000), *vol.* 416, *pp.* 45–73. Printed in the United Kingdom

Numerical investigation of transitional and weak turbulent flow past a sphere

By ANANIAS G. TOMBOULIDES[1] AND STEVEN A. ORSZAG[2]

[1] Department of Aerospace and Mechanical Engineering, Boston University, 110 Cummington Street, Boston, MA 02215, USA

[2] Department of Mathematics, Yale University, P.O. Box 208283, New Haven, CT 06510-8283, USA

(Received 26 April 1999 and in revised form 3 January 2000)

This work reports results of numerical simulations of viscous incompressible flow past a sphere. The primary objective is to identify transitions that occur with increasing Reynolds number, as well as their underlying physical mechanisms. The numerical method used is a mixed spectral element/Fourier spectral method developed for applications involving both Cartesian and cylindrical coordinates. In cylindrical coordinates, a formulation, based on special Jacobi-type polynomials, is used close to the axis of symmetry for the efficient treatment of the 'pole' problem. Spectral convergence and accuracy of the numerical formulation are verified. Many of the computations reported here were performed on parallel computers. It was found that the first transition of the flow past a sphere is a linear one and leads to a three-dimensional steady flow field with planar symmetry, i.e. it is of the 'exchange of stability' type, consistent with experimental observations on falling spheres and linear stability analysis results. The second transition leads to a single-frequency periodic flow with vortex shedding, which maintains the planar symmetry observed at lower Reynolds number. As the Reynolds number increases further, the planar symmetry is lost and the flow reaches a chaotic state. Small scales are first introduced in the flow by Kelvin–Helmholtz instability of the separating cylindrical shear layer; this shear layer instability is present even after the wake is rendered turbulent.

1. Introduction

Extensive steady-state axisymmetric numerical simulations of flow past a sphere were reported by Fornberg (1988), who observed that the wake length and separation angle vary approximately as $\log(Re)$ for Reynolds number, Re, greater than about 75. Experimental results for flow past a sphere have been reported by Taneda (1956) and Nakamura (1976), for Re up to approximately 200; these experiments report that a closed recirculation zone first forms at approximately $Re = 20$–25 and the flow stays steady and axisymmetric up to at least Re of about 130 (Taneda 1956). Taneda (1956) found wake unsteadiness above $Re = 130$. Other more recent experimental observations (Wu & Faeth 1993; Magarvey & Bishop 1965) find the flow to be steady and axisymmetric up to $Re \approx 210$.

Linear stability analysis results (Kim & Pearlstein 1990) suggest that the first transition of the flow past a sphere occurs at Re of about 175 and is a Hopf bifurcation characterized by a low frequency. This result disagrees with more recent

LSA results by Natarajan & Acrivos (1993), who found that the first transition of this flow occurs at $Re_1 = 210$ and is of the 'exchange of stability', or *regular* bifurcation, type. In contrast to the flow past a circular cylinder where the first transition is a Hopf bifurcation from a two-dimensional steady to a two-dimensional unsteady (periodic) flow (resulting in a time-periodic Kármán vortex street), this transition is from an axisymmetric steady to a three-dimensional steady flow. The most unstable azimuthal mode is the first azimuthal mode. The characteristics of the resulting steady flow field, which exists and is stable for Re between approximately 210 and 270, correspond to those of a 'double-threaded' wake, reported in the falling sphere experiments of Magarvey & Bishop (1965) and Nakamura (1976). The double-threaded wake consists of two streamwise vortices opposite in sign which extend to infinity and appear in the experiment as two dye threads emanating from the end of the recirculation region. Its effect is most easily demonstrated by the curved non-vertical path of a sphere falling in a quiescent fluid. In this range of Re, the flow is symmetric around a plane that includes the axis of symmetry, but the flow is not axisymmetric. This planar symmetry is also maintained at higher Reynolds numbers; its precise orientation is random, presumably determined by perturbations in the incoming flow.

Natarajan & Acrivos (1993) find that at $Re_2 = 277.5$ a second mode becomes unstable, always with respect to the steady axisymmetric flow. From their work, it is evident that there exist two eigenvalues, one with zero and another one with non-zero frequency, which are well separated from the rest of the spectrum of the first azimuthal mode $m = 1$. The former eigenvalue crosses the imaginary axis at Re_1, whereas the latter becomes supercritical at Re_2. This latter mode is stable below Re_2 but it may be related to low-amplitude sustained oscillations, without distinct vortex shedding, often reported in experiments below $Re = 270$. Such wave-like oscillations have been reported by Möller (1938) for $Re \geqslant 200$, by Magarvey & Bishop (1965) for $270 \leqslant Re \leqslant 290$, and in the experimental work of Sakamoto & Haniu (1990, 1995) for $Re < 300$. This second instability was also investigated experimentally by Provansal & Ormières (1998) and Ormières, Provansal & Barrantes (1998), who attempted to quantify the Landau equation exponents for this transition by performing water tunnel visualization experiments. Recently, Johnson & Patel (1999), have performed both experiments and numerical simulations based on a finite volume scheme for Re up to 300 and found results that are in agreement with these observations.

Experimental observations at higher Re (just above 300) suggest that the flow becomes time periodic. The basic wake structure consists of a succession of interconnected vortex loops as observed in visualization experiments by Magarvey & Bishop (1961), Achenbach (1974) and Sakamoto & Haniu (1990). In particular, Achenbach (1974) reports that the flow at about $Re = 300$ maintains planar symmetry around the plane on which the shedding process is initiated, even though it has lost its axial symmetry. To demonstrate this, he includes a sketch which shows that the vortex loops are always shed from the sphere with the same orientation.

Sakamoto & Haniu (1990, 1995) report that the flow undergoes another transition from a one-frequency to an almost chaotic system for $Re > 420$. In his experiments, Achenbach (1974) reports two values for the Strouhal number at $Re = 500$, corresponding to two different spheres and blocking ratios; the first is about 0.163 and corresponds to a blockage of about 0.6% and the second is about 0.174 and corresponds to blockage of about 2.6%. His experiments were performed in a round pipe, like our simulations. Kim & Durbin (1988) report a Strouhal number of 0.171

for $Re = 500$ and their blockage ratio is less than 0.01% for this Reynolds number; their experiments were performed in a wind tunnel of rectangular cross-section. Finally, Sakamoto & Haniu (1990) find a Strouhal number between 0.175 and 0.18 for $Re = 500$. Some three-dimensional simulations in this Re range are reported by Shirayama (1992), and Gebing (1994) for compressible flow at Mach number of 0.4.

Experimentally, smaller scales appear and a more chaotic flow occurs when the Reynolds number exceeds 800. The basic wake structure seems to be similar to the one at $Re = 500$; however, a Kelvin–Helmholtz-like instability of the cylindrical shear layer that results from the separation of the boundary layer on the sphere creates an additional instability mode with a different characteristic frequency. In the experiments of Kim & Durbin (1988), two frequencies are reported for around $Re > 800$. At $Re = 1000$, the lower frequency is found to be between 0.187 and 0.202 and the higher frequency mode is measured to be between 0.33 and 0.37 (see figure 2 in Kim & Durbin 1988). In his experiments, Achenbach (1974) regarded all the observed frequencies as being due to vortex shedding and only measured the higher Strouhal frequency mode. He reports a Strouhal number of about 0.39 at $Re = 1000$. Sakamoto & Haniu (1990, 1995) report a value between 0.195 and 0.205 for the vortex shedding Strouhal number, and a value of about 0.29–0.34 for the second higher mode. Since the second frequency is associated with the instability of the shear layer, it tends to increase with Reynolds number, or equivalently with decreasing thickness of the layer, because the shear layer becomes unstable to smaller wavelengths. The frequency was found by Kim & Durbin (1988) to increase as $Re^{0.75}$. Finally, average and RMS velocity profiles were measured by Wu & Faeth (1993) for Re up to 960.

The current work is concerned with the computational investigation of viscous incompressible flow past a sphere. The approach we have taken is the detailed study of the underlying physical mechanisms of the transition to turbulence for this prototypical wake flow, using direct numerical simulation (DNS) based on spectral-type methods. A mixed spectral element/Fourier spectral method is used, which takes advantage of the homogeneity in the azimuthal direction in cylindrical coordinates, or in the spanwise direction in Cartesian coordinates. An approach based on special Jacobi-type polynomials is used on the axis of symmetry for the treatment of the 'pole' problem in cylindrical coordinates. This approach, when used in the context of spectral elements, leads to an efficient and spectrally accurate way of removing geometrical singularities and can be used for the simulation of three-dimensional flows in general axisymmetric geometries. A description of the numerical formulation used in this work is given in the following section.

Results from our investigation of the flow past a sphere, for Re from 25 up to 1000, are reported. The Reynolds number is defined in terms of the diameter of the sphere, D, the free-stream velocity, U_o, and the kinematic viscosity, ν. Therefore, all length scales are non-dimensionalized by D, all velocities by U_o, and all time scales by D/U_o. The results are presented for increasing Reynolds number, starting from steady axisymmetric flow. The first transition that the flow undergoes from axisymmetry to three-dimensionality is analysed both in terms of its early stages and in terms of the final resulting flow field. Extensive comparisons with results from linear stability analysis and experiments are performed. The transition to time dependence and onset of vortex shedding is successfully uncovered and simulated. Shedding patterns, the appearance of small scales, and the onset of turbulence are thoroughly investigated and compared with experiments.

2. Numerical formulation

The governing equations are the incompressible Navier–Stokes equations, which in rotational form are

$$\frac{\partial \boldsymbol{v}}{\partial t} + \omega \times \boldsymbol{v} = -\nabla P + \nu \nabla^2 \boldsymbol{v} \tag{2.1a}$$

$$\nabla \cdot \boldsymbol{v} = 0 \text{ in } \Omega, \tag{2.1b}$$

where $\boldsymbol{v} = (u, v, w)$ is the velocity field (where u, v, w refer to streamwise, radial and azimuthal velocity components, respectively), $P = p + \frac{1}{2}\boldsymbol{v} \cdot \boldsymbol{v}$ is the total pressure, $\omega = \nabla \times \boldsymbol{v}$ is the vorticity, and ν is the kinematic viscosity. The discretization of the equations is performed using spectral methods and employs a Fourier series expansion in the azimuthal direction:

$$u(z, r, \phi, t) = \sum_{m=0}^{M-1} u_m(r, z, t) \mathrm{e}^{\mathrm{i}m\phi}, \tag{2.2}$$

where m represents azimuthal Fourier modes. Substituting (2.2) in the governing equations, and applying the change of variables

$$\tilde{v}_m = v_m + \mathrm{i}w_m, \quad \tilde{w}_m = v_m - \mathrm{i}w_m, \tag{2.3}$$

gives

$$\frac{\partial u_m}{\partial t} + \mathscr{F}_m(\omega \times \boldsymbol{v})_z = -\frac{\partial P_m}{\partial z} + \nu \left(\nabla_{rz}^2 - \frac{m^2}{r^2} \right) u_m, \tag{2.4a}$$

$$\frac{\partial \tilde{v}_m}{\partial t} + \tilde{\mathscr{F}}_m(\omega \times \boldsymbol{v})_r = -\left(\frac{\partial P_m}{\partial r} - \frac{m}{r} P_m \right) + \nu \left(\nabla_{rz}^2 - \frac{(m+1)^2}{r^2} \right) \tilde{v}_m, \tag{2.4b}$$

$$\frac{\partial \tilde{w}_m}{\partial t} + \tilde{\mathscr{F}}_m(\omega \times \boldsymbol{v})_\phi = -\left(\frac{\partial P_m}{\partial r} + \frac{m}{r} P_m \right) + \nu \left(\nabla_{rz}^2 - \frac{(m-1)^2}{r^2} \right) \tilde{w}_m, \tag{2.4c}$$

where

$$\nabla_{rz}^2 = \frac{\partial^2}{\partial z^2} + \frac{1}{r}\frac{\partial}{\partial r}\left(r \frac{\partial}{\partial r} \right),$$

$$\tilde{\mathscr{F}}_m(\omega \times \boldsymbol{v})_r = \mathscr{F}_m(\omega \times \boldsymbol{v})_r + \mathrm{i}\mathscr{F}_m(\omega \times \boldsymbol{v})_\phi,$$

$$\tilde{\mathscr{F}}_m(\omega \times \boldsymbol{v})_\phi = \mathscr{F}_m(\omega \times \boldsymbol{v})_r - \mathrm{i}\mathscr{F}_m(\omega \times \boldsymbol{v})_\phi,$$

and $\mathscr{F}_m$ refers to a Fourier transform in ϕ. The coordinate singularity at $r = 0$ is removable, since it can be shown that the behaviour of the Fourier coefficients of the velocity components close to the axis is

$$(u_m, v_m, w_m) \propto (\beta r^m, \gamma r^{m-1}, \mathrm{i}\gamma r^{m-1}), \tag{2.5}$$

where β and γ are constants (Orszag 1974; Batchelor 1967). It can be verified that $\tilde{v}_m = v_m + \mathrm{i}w_m$ is zero at $r = 0$ for all m and scales like $v_m + \mathrm{i}w_m \propto r^{m+1}$, a result equivalent to the fact that the vorticity is regular at $r = 0$. On the other hand, the variable $\tilde{w}_m = v_m - \mathrm{i}w_m$ has a non-zero value at $r = 0$ for $m = 1$; however, the coefficient of the $1/r^2$ terms in (2.4c) for $m = 1$ is zero and so the singularity is removed.

Numerically, however, there are still terms in the equations where both the numerator and the denominator go to zero at the same rate close to the axis, which means that quantities of indeterminate form have to be treated. To do this, a special form

of Jacobi polynomials is used as an expansion basis in the r-direction adjacent to the axis, which in conjunction with L'Hôpital's rule results in a removal of the geometrical singularity, thus preserving the spectral convergence rate (E. Rønquist 1991, personal communication; Leonard & Wray 1982). The set of polynomials employed close to the axis correspond to the Jacobi polynomials $P^{(0,1)}$, with associated weights which are zero at $r = 0$.

For the time integration of (2.4*a*), (2.4*b*), (2.4*c*), we use a fractional step method, in conjunction with a mixed explicit/implicit stiffly stable scheme of second order of accuracy in time (Karniadakis, Israeli & Orszap 1991). A consistent Neumann boundary condition is used for the pressure, based on the rotational form of the viscous term, which nearly eliminates splitting errors at solid (Dirichlet) velocity boundaries (Tomboulides, Israeli & Karniadakis 1989). The resulting Helmholtz equation is of the form

$$\frac{1}{r}\frac{\partial}{\partial r}\left(r\frac{\partial}{\partial r}u_m\right) - \frac{m^2}{r^2}u_m - \lambda^2 u_m = g, \tag{2.6}$$

where u_m stands for either the velocity or pressure Fourier mode, and m is an azimuthal wavenumber. The constant λ^2 is 0 for the pressure and $\gamma_0/(\nu\Delta t)$ for the velocity equations (γ_0 being a coefficient associated with the order of the time-integrating scheme used).

The spatial discretization of the Helmholtz equation (2.6) is performed using two-dimensional spectral elements (Patera 1984; Maday & Patera 1987). In the elements adjacent to the axis of symmetry we use Lagrange interpolants based on zeros of Jacobi (0, 1) polynomials, whereas in the rest of the elements Legendre–Lagrangian interpolants are employed (Tomboulides 1993). The resulting matrices for the numerical solution of the two-dimensional Helmholtz equations (2.6), are essentially block diagonal and can be solved efficiently by a static condensation technique (with operation count approximately $M \times K_e \times N^2$, where N is the number of grid points inside a single element and K_e the total number of elements (typically $K_e \leqslant 200$ and $N \leqslant 15$). This approach was used only for the zeroth-pressure Fourier mode P_0 because of slow convergence properties when iterative techniques were used. The Helmholtz equations for the rest of the unknowns, i.e. all P_m, for $m \neq 0$ and all velocity modes, were solved using preconditioned conjugate gradient iterative solvers. The code is fully parallelized and most high-Re computations were performed on an IBM PVS parallel computer.

A demonstration of the accuracy and convergence rate of the present methodology for axisymmetric geometries is given in figure 1 in terms of the logarithm of the maximum error in the vorticity along the axis for the flow past a sphere at $Re = 25$, as the polynomial order N of the discretization is increased. The vorticity along the axis for an axisymmetric flow is zero; this condition, however, is not imposed strongly, but is satisfied naturally through the convergence process. It can be observed in figure 1 that the convergence of the error with increasing polynomial order is exponential.

2.1. *Simulation parameters*

The simulations were performed on a mesh which extends 4.5 diameters upstream and radially outwards from the centre of the sphere, corresponding to a blockage (area) ratio of about 1.2%. The boundary condition at the upstream and outer radial boundaries is a constant streamwise velocity of $U_o = 1$, with the sphere being stationary. This is equivalent to the sphere being towed inside a circular pipe with diameter $\mathscr{D} = 9\,D$ (where D is the diameter of the sphere). The radial and upstream

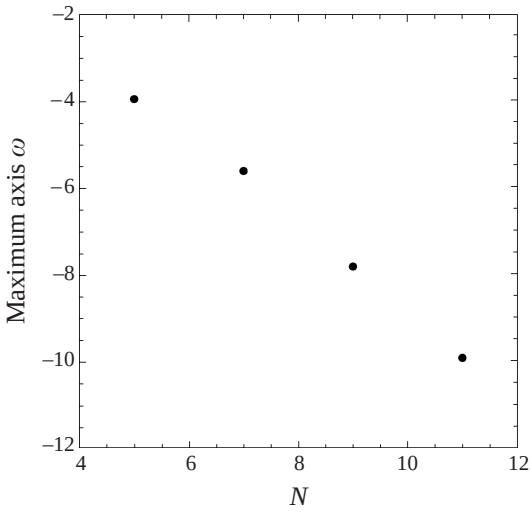

FIGURE 1. Convergence of maximum vorticity along the axis to zero for flow past a sphere at $Re = 25$ with order N.

extent of the computational domain was selected by considering the rate at which perturbations decay away from the body. It is well known (Batchelor 1967) that perturbations due to the existence of the sphere decay away from the sphere at a rate $1/r^3$, where r is the distance from the centre of the sphere. This is a factor of r smaller than the corresponding decay of perturbations due to a two-dimensional body (i.e. a circular cylinder) which is $1/r^2$. As a result, at $x = -4.5$ the velocity is only 0.1% different from the free-stream velocity, according to potential theory. The same argument also holds in the radial direction. In addition, blockage factors of the order of 1% are considered negligible when performing experiments for this flow, as mentioned by Kim & Durbin (1988) and Achenbach (1974).

In the downstream direction the computational domain extends 25 diameters from the sphere centre. The boundary conditions used at the downstream boundary are of outflow type, Neumann on velocity components and Dirichlet for the pressure, as described in Tomboulides (1993). The Neumann boundary conditions for the velocity components are only enforced in the weak sense, and the streamwise derivatives of the velocity components at the outflow boundary do not have to be identically zero. This is the main reason why this type of outflow boundary condition works well with methods based on the variational formulation and does not generate numerically induced oscillations. On the other hand, the Dirichlet condition on the pressure, i.e. $p = 0$ at the outflow, is equivalent to setting the normal component of the stress tensor to zero at the outflow ($-p + 2\mu\partial u/\partial n \approx -p = 0$, for small values of the viscosity), as described in Gresho & Sani (1987). Numerical experiments were performed with both types of conditions on the pressure and the results upstream were virtually unchanged. An alternative approach based on the parabolized equations, in a sponge layer close to the outflow, was also employed and again the results outside this sponge layer were not affected. Simulations with a domain length of 20 diameters were also performed and it was found that the outflow boundary did not have any effects upstream. The main reason for extending the domain to 25 diameters was to have a minimum of 3 to 4 vortical structures shed from the sphere within the domain.

The z, r projection of a typical spectral element mesh used for the simulations

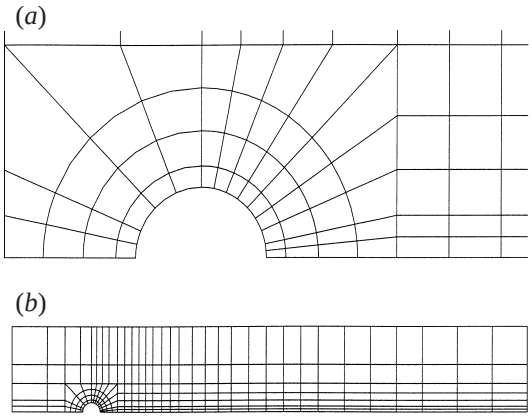

FIGURE 2. Typical SEM mesh for flow past a sphere consisting of 246 elements: (*a*) elements close to the sphere, (*b*) complete mesh.

reported here is plotted in figure 2, which consists of 246 elements. The three-dimensional domain is obtained by a 360° rotation of the mesh shown in that figure. The close-up of the element arrangement close to the sphere shows the increased resolution in that area, chosen to resolve the steepening of the boundary layer. The number of points inside all elements was either 7×7, for the low-Re axisymmetric simulations, 9×9 for all three-dimensional simulations up to $Re = 500$ and 11×11 for most simulations at $Re = 1000$. The resolution used was more than adequate to resolve all scales, both in the boundary layer and in the near wake, at all Re. Two measures of accuracy were considered in order to locally increase resolution when needed by adding more elements or by increasing the number of collocation points within each element. One is the total L_2 divergence of the velocity field, which is a measure of how well the velocity gradients are captured. This value was maintained below 10^{-4} for all simulations. Another measure is the vorticity, which at low resolutions contains jumps at element boundaries. The only case where resolution was marginal was at $Re = 1000$; however, we believe that our simulations do capture the details of the flow both qualitatively and quantitatively.

The number of azimuthal angle increments (double the number of Fourier modes) used was 16 for simulations up to $Re = 300$, and was doubled to 32 for the rest of the simulations up to $Re = 500$. All three-dimensional simulations up to $Re = 500$ were initialized with the steady axisymmetric flow corresponding to the same Reynolds number together with a perturbation in the $m = 1$ Fourier mode. The simulation at $Re = 1000$ was restarted from the results of the $Re = 500$ run and the number of azimuthal angle increments used in the early stages of this computation was 32; however, soon after the energy in the high end of the spectrum started increasing due to the generation of smaller scales and in order to maintain at least 4 decades of decay in the spectrum the resolution in the azimuthal direction for this Re was doubled to 64. With this increase the tail of the energy spectrum is reduced by at least a factor of 10^{-4}, and that of the dissipation is reduced by at least a factor of 10^{-3} or so, which experience has proven to be adequate to provide confidence in our results. After that the simulation proceeded without need for any further refinement.

Since the boundary layer on the sphere does not become turbulent until a Reynolds number of the order of 3×10^5 (based on the diameter) is reached, estimates of the boundary layer thickness were derived from the laminar boundary layer solution

Re	100	300	500	1000
δ	0.113	0.065	0.05	0.035
L_{req}	0.8	0.46	0.35	0.25
L_{used}	0.167	0.167	0.167	0.15

TABLE 1. Boundary layer and element thickness.

Re	25–300	500	1000
Δt	0.005	0.003	0.0025

TABLE 2. Time steps used for simulations at different Reynolds number.

for axisymmetric bodies (Schlichting 1979). Values of the smallest boundary value thickness for Reynolds numbers from 100 to 1000 are given in table 1 together with an estimate of the element thickness required for adequate resolution of the gradient there, L_{req}, was obtained using the estimate $N \approx 3/\sqrt{\delta/L}$ (Gottlieb & Orszag 1977), for a polynomial degree 9.

Also shown in the third row of the matrix is the actual thickness of the layer of elements which contains the boundary layer. It can be concluded from the table that the mesh size used close to the boundary layer was small enough to accurately resolve it for all Reynolds numbers. The computed thicknesses of the boundary layers for all cases were very close to the estimates given in table 1. The tolerance used for the iterative conjugate gradient solvers of the pressure (for modes other than 0) was less than 10^{-5} for most of the simulations, whereas the corresponding tolerance for the velocities was always set to 10^{-7}. Overall in all simulations, mass conservation was always satisfied to below 10^{-6} in the average value of the divergence and to 10^{-4} in L_2 norm. The momentum conservation was also globally conserved to 10^{-5}.

A second-order mixed stiffly stable scheme was used for the time integration of the equations and the time steps used for all simulations are summarized in table 2. As a test for the time accuracy of the simulations, the $Re = 300$ simulation was performed as follows: a time step of 0.005 was used until a single-frequency limit cycle was obtained. Then, the time step was reduced to 0.0025 and the simulation was continued and the Strouhal number was measured again with the new time step. It was found that the difference in the value of the Strouhal number was less than 0.1%. Since this difference is fairly small, the criteria for the selection of the time step for each Re were dominated almost entirely by issues relevant to numerical stability (i.e. the CFL condition) rather than accuracy. In addition, the time step used for the high Reynolds number simulations was at least an order of magnitude smaller than the time scales corresponding to the highest frequencies of the flow, as discussed in the following sections.

The flow past a sphere was investigated numerically, and computational results are presented for Reynolds numbers from $Re = 25$ to 1000 using direct numerical simulation (DNS) based on spectral-type methods. The results are organized in increasing Reynolds number order, in the following way: in the first of the following sections, the low Reynolds number axisymmetric flow results are presented, whereas the next subsection contains the early transitional results between Reynolds number 212 and 270. Direct simulations that correspond to flow with vortex shedding, from $Re = 285$ to 1000 are presented last. Most of the results presented here are reported in Tomboulides (1993).

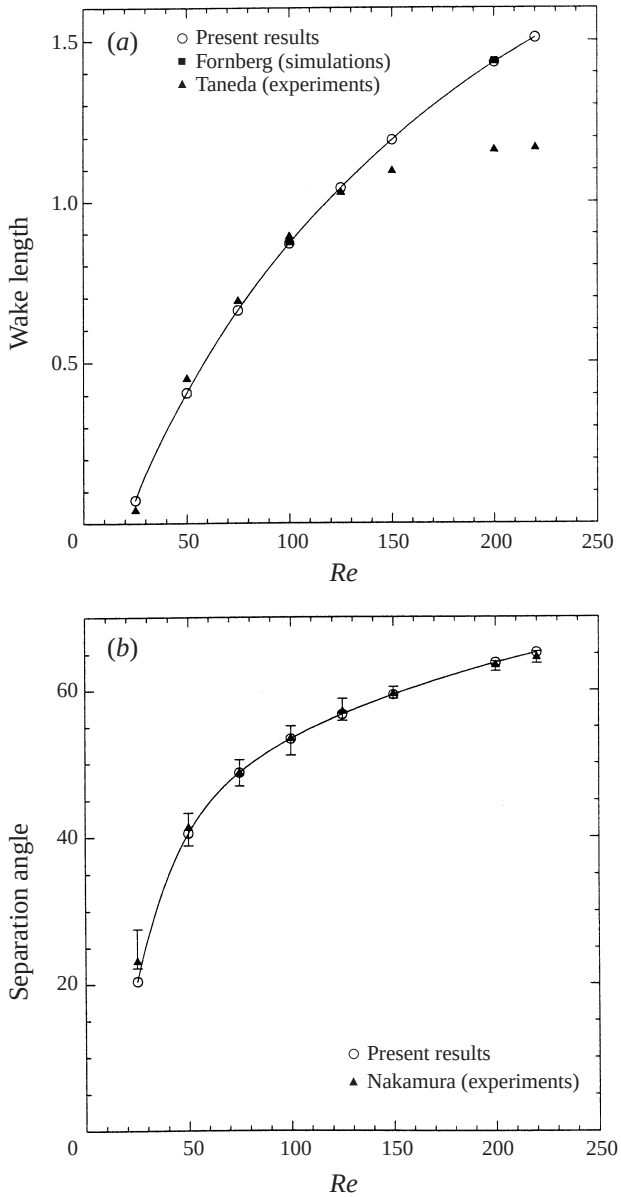

FIGURE 3. (*a*) Wake length and (*b*) separation angle with respect to Reynolds number.

3. Axisymmetric flow

Our simulations reveal that the flow past a sphere is axisymmetric up to a Reynolds number of approximately 212. Results from axisymmetric numerical simulations up to $Re = 220$ are shown in figures 3(*a*), and 3(*b*), where the wake length and separation angle are plotted with respect to the Reynolds number. Both the wake length and the separation angle are measured from the rear stagnation point of the sphere; the wake length is normalized by the sphere diameter. It can be extrapolated from the figure that a recirculation region does not exist below a Reynolds number of about 20. Both quantities follow an approximately logarithmic relationship with the Reynolds

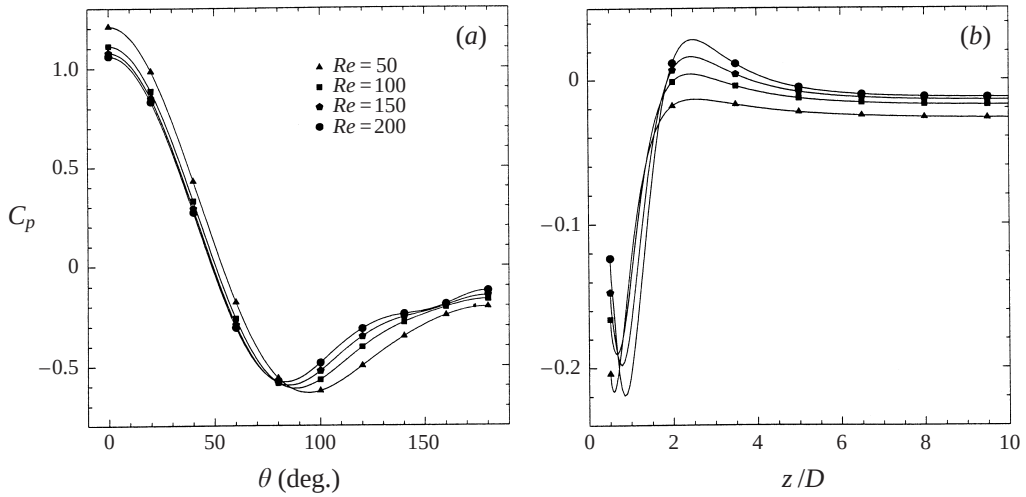

FIGURE 4. Pressure coefficient C_p: (*a*) along the surface of the sphere, (*b*) along the axis, from the rear end of the sphere.

number for Re greater than about 75, as previously observed by Fornberg (1988). The results up to $Re = 220$ agree with the numerical results of Fornberg (1988) to 0.3–0.5% in terms of wake length, and up to 2% in terms of the drag coefficient. The agreement with the experimental results of Taneda (1956) and Nakamura (1976) is also good. The discrepancy in the values of the wake length for $Re > 130$ in figure 3(*a*) can be explained by the fact that Taneda (1956) has reported wake unsteadiness above $Re = 130$, whereas our simulations and other experiments, e.g. Wu & Faeth (1993) and Magarvey & Bishop (1965), find the flow to be steady and axisymmetric up to $Re \approx 210$. Taneda's wake length results are used for comparison with our numerical results only because they are the only experimental results where wake length measurements are reported.

Another interesting feature of the flow is the pressure coefficient, defined as

$$C_p = \frac{p - p_o}{\frac{1}{2}\rho U_o^2}, \tag{3.1}$$

where p_o and U_o are the pressure and the velocity of the incoming flow at infinity. The distribution of C_p along the surface of the sphere is plotted in figure 4(*a*) for various values of the Reynolds number, and in figure 4(*b*) along the streamwise direction, starting from the rear end of the sphere. The detailed values of the pressure coefficient C_{pb} at the rear end of the sphere (base pressure coefficient) for different Reynolds number are plotted in figure 5.

4. Transition to non-axisymmetric flow

According to our simulations, at approximately $Re = 212$ the flow past a sphere undergoes a transition to three-dimensionality through a *regular* bifurcation. The most unstable azimuthal mode is $m = 1$. This first transition has zero frequency associated with it, in agreement with Natarajan & Acrivos (1993), who report results of linear stability analysis on this flow. Three-dimensional simulations were performed at Reynolds numbers 200, 220, 250, 270, 285, and 300. For all simulations, the axisymmetric steady flow was computed first. This flow was used as an initial condition for a

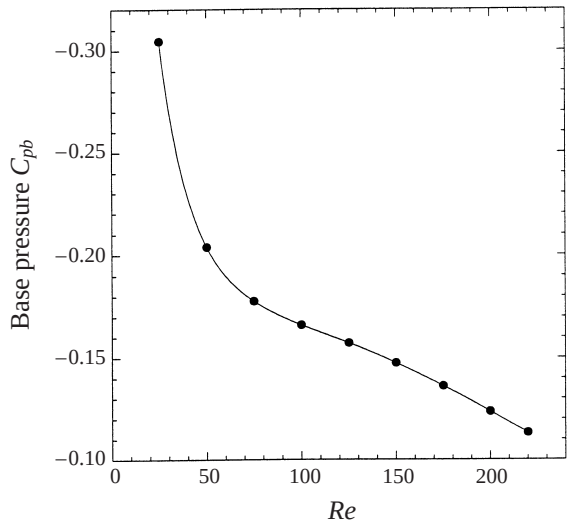

FIGURE 5. Base pressure coefficient C_{pb} as a function of Re.

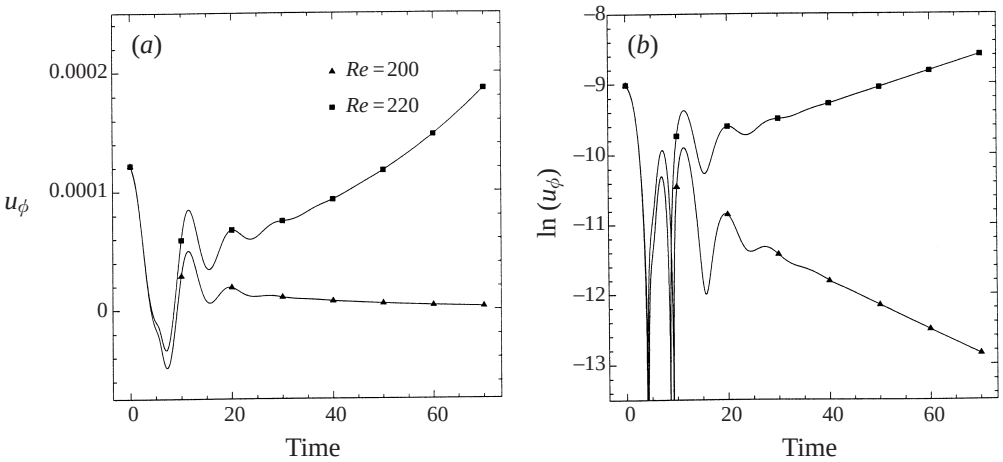

FIGURE 6. (*a*) Time history of $m = 1$ of u_ϕ at $z = 1D, r = 0.2D$.
(*b*) As (*a*) but in log-linear coordinates.

three-dimensional simulation, together with a perturbation of total energy 10^{-8} in the first $m = 1$ azimuthal mode. This perturbation was random, so that the initial energy in the whole eigenspectrum of mode $m = 1$ was guaranteed. The initial condition was then marched in time, and the energy of all azimuthal modes was tracked in time.

From the six cases mentioned above, only at $Re = 200$ does the energy of the first mode decay in time, and that flow eventually returns to axisymmetry. For $Re \geqslant 220$, the $m = 1$ mode is always unstable. In figure 6(*a*), the time history of the azimuthal velocity u_ϕ of the first Fourier mode is plotted at a point in the near wake, showing the final exponential decay of the first mode for $Re = 200$, and its exponential growth at the same point for $Re = 220$. The same plot, in logarithmic versus linear coordinates, is given in figure 6(*b*), where the linear part of the decay (or growth) can be observed more easily. The fact that the small initial perturbation in the $m = 1$ mode grows

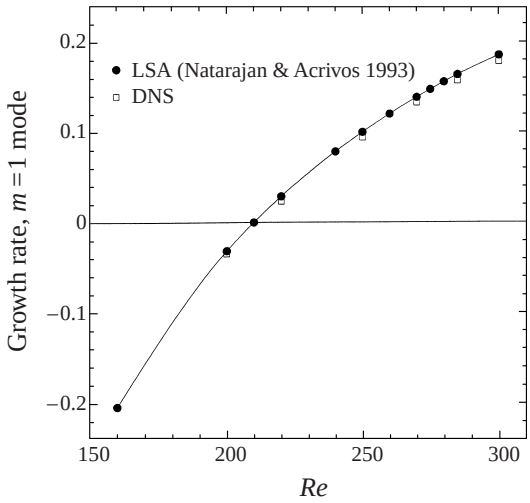

FIGURE 7. Growth rate of the least stable $m = 1$ mode with Re.

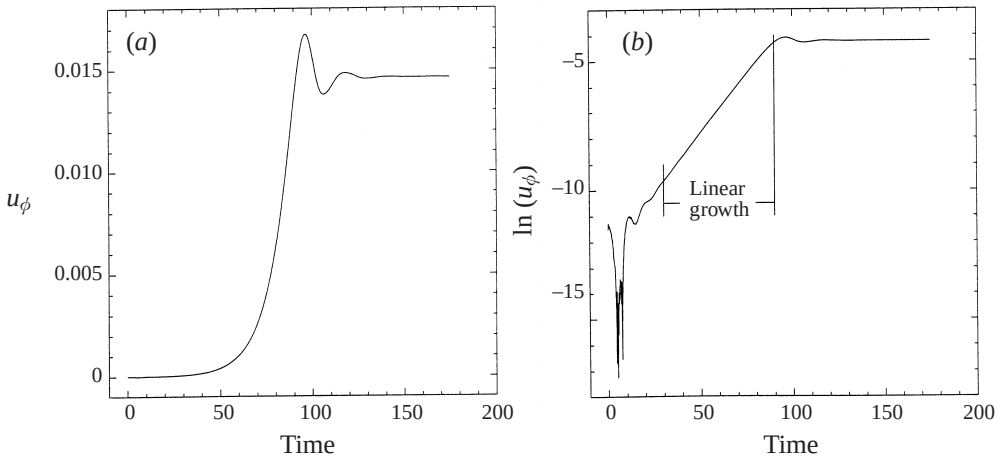

FIGURE 8. (*a*) Time history of the $m = 1$ mode of u_ϕ at $(1.0D, 0.2D)$, $Re = 250$. (*b*) As (*a*) but in long-linear coordinates.

exponentially after the effect of the initial conditions is washed out implies that the first transition of the flow past a sphere is a 'linear' transition, in contrast to prototype wall-bounded flows (i.e. in a channel or pipe), where finite-amplitude effects give rise to transition.

In figure 7 we plot a comparison of our numerical results of the growth rate of this mode and the results of Natarajan & Acrivos (1993); the growth (or decay) rates were measured for each case from the slope of the straight line segment in log-linear coordinates. The first instability occurs at $Re = 210$ as reported by Natarajan & Acrivos (1993), and at approximately $Re = 212$ for the current numerical results; the two values differ by less than 1%. The growth rates found by the two methods differ by a maximum of about 5%. Results from a simulation at $Re = 250$, are shown in figures 8(*a*) and 8(*b*), where the time history of the $m = 1$ mode of the azimuthal velocity is plotted at a point in the near wake of the sphere. After the stages of exponential growth (associated with the linear mode) and nonlinear saturation, a

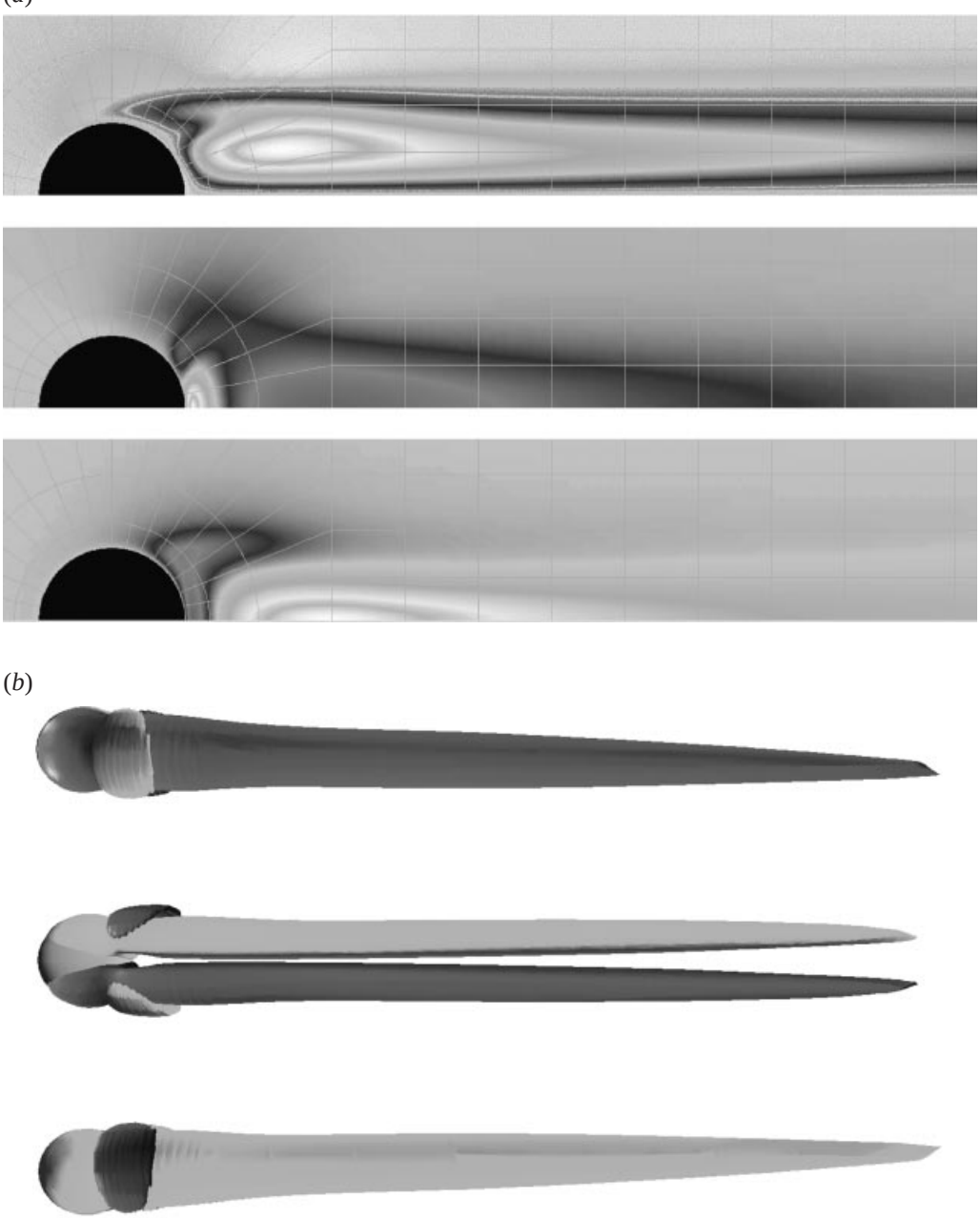

FIGURE 9. (*a*) Isocontours of u_z, u_r, u_ϕ, for the unstable $m = 1$ mode at $Re = 250$, from DNS. (*b*) Isosurfaces of streamwise vorticity.

three-dimensional steady-state solution is finally achieved. In addition, the shape of the $m = 1$ mode during the stages of 'linear growth' (see figure 8(*b*)) is in remarkable agreement with the least stable $m = 1$ mode shape as reported by Natarajan & Acrivos (1993). In figure 9(*a*) we plot isocontours of the streamwise, radial and azimuthal velocities associated with the $m = 1$ mode at $Re = 250$. The same isocontours as calculated by linear stability are given by Natarajan & Acrivos (1993) and are very similar to the ones shown in figure 9(*a*).

The characteristics of the resulting steady flow field, which exists and is stable up to a Reynolds numbers of approximately 270, correspond to that of the 'double-thread' wake, reported in falling sphere experiments (Magarvey & Bishop 1965), which exists between Reynolds numbers of 210 and 270. The double-thread wake consists of two opposite-sign streamwise vortices which extend to infinity and appear in the experiment as two dye threads emanating from the end of the recirculation region. It is also characterized by a loss of axisymmetry in the path of the falling sphere (Magarvey & Bishop 1965). The computed three-dimensional steady flow field for $Re = 250$ is shown in figure 9(b), in terms of streamwise vorticity isocontours. The dark and light colours specify values of streamwise vorticity, equal in magnitude but opposite in sign respectively. The three views shown in figure 9(b) differ by 90° with respect to one another. It can be observed from this plot that the flow is symmetric around a plane that includes the axis of symmetry, but it is not axisymmetric. This planar symmetry is also maintained at higher Reynolds numbers. In experiments on this flow, the plane of symmetry is sensitive to external disturbances which control its actual location. In the simulations, the fact that the initial perturbation of the $m = 1$ azimuthal mode is real fixes the phase of this mode and determines the location of the symmetry plane.

During the early stages of the first transition, an oscillatory subdominant mode is observed, together with the dominant zero-frequency $m = 1$ mode. This second $m = 1$ mode decays for all $Re \leqslant 270$ and only the first dominant mode exists in the later stages of the transition below that Reynolds number. The existence of such a mode was first reported in the linear stability analysis study of Natarajan & Acrivos (1993). From their work, it is evident that there exist two eigenvalues, one with zero and another one with non-zero frequency, which are well separated from the rest of the spectrum of the first azimuthal mode $m = 1$. The former eigenvalue crosses the imaginary axis at $Re = 210$, whereas the latter, always with respect to the base axisymmetric flow, becomes supercritical at $Re = 277.5$. The magnitudes of the eigenvalues, for both of these modes, are given in Natarajan & Acrivos (1993) for the range $160 \leqslant Re \leqslant 300$. In figure 10, we plot the time history of the $m = 1$ azimuthal component of the velocity at location ($z = 2D$, $r = 0.3D$) in the wake of the sphere for Reynolds numbers between 200 and 300. All simulations started with the same type and magnitude of perturbation in the $m = 1$ azimuthal mode added to the corresponding steady axisymmetric flow field. It can be observed from this figure that oscillations with a characteristic frequency develop from the initial conditions and decay for $Re \leqslant 270$, whereas they grow for $Re \geqslant 285$. The approximate values of the frequencies for each of these cases are given in table 3 and are in reasonably good agreement with the corresponding values reported in Natarajan & Acrivos (1993) for the subdominant mode, also given in the table.

In order to isolate the subdominant oscillatory mode, it is necessary to subtract the dominant mode from the time history of the $m = 1$ mode, which contains both of them. This was accomplished by subtracting a function of the form $\alpha(e^{\sigma t} - 1)$ from the total time trace, where σ is the measured dominant-mode growth rate, and α is a locally measured amplitude. For example, in figure 11(a), we plot the time history of the $m = 1$ azimuthal velocity component at point ($z = 2D, r = 0.3D$) for $Re = 300$, indicating the possible coexistence of two modes, one monotonically increasing in amplitude and a second oscillatory one. The measured value of the growth rate of the dominant mode for $Re = 300$ is 0.178, and the time variation of this mode only is shown as a dotted line in the same plot. The resulting time trace after subtracting the second curve from the first is shown in figure 11(b), demonstrating the increasing

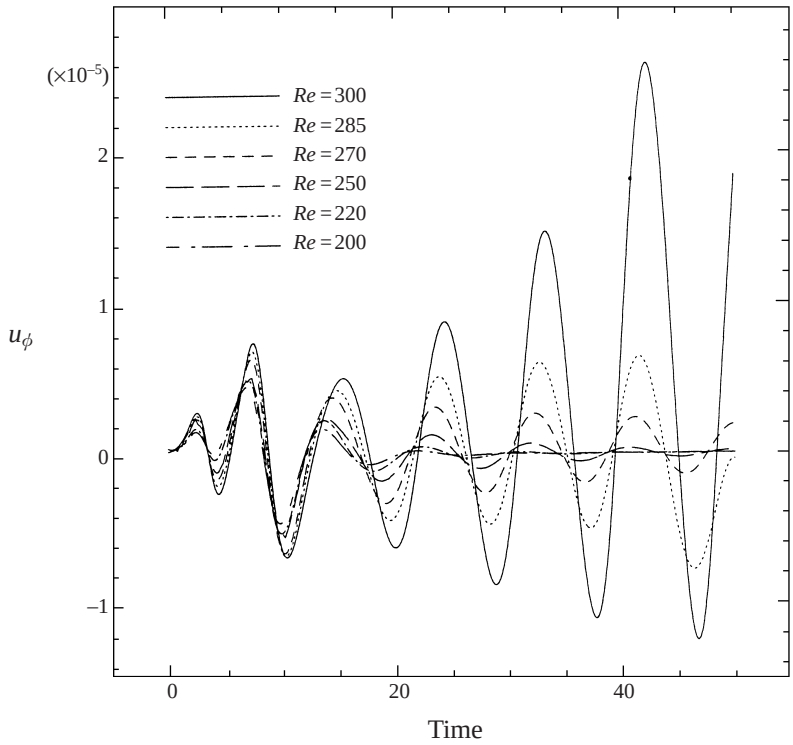

FIGURE 10. Time history of the $m = 1$ mode of u_ϕ at $(2.0D, 0.3D)$ vs. Re.

Re	200	220	250	270	300
St_L (present work)	0.1178	0.1154	0.1132	0.1128	0.1121
St_L (Natarajan & Acrivos 1993)	0.1181	0.1157	0.11365	0.11305	0.11335

TABLE 3. Frequencies St_L of subdominant $m = 1$ azimuthal mode, linear stage.

amplitude of the oscillatory mode. The growth rate of this mode can only be measured approximately; however it is close to the values reported in Natarajan & Acrivos (1993) for the whole range of Reynolds numbers between 200 and 300. In fact, this growth rate with respect to the base axisymmetric flow, when non-dimensionalized using D/U_o, was found to depend approximately linearly on $(Re - Re_2)/Re_2$, where Re_2 is the critical Re for the second transition (approximately equal to 277.5), with a proportionality constant between 0.7 and 0.9. Ormières *et al.* (1998) found the growth rate for this oscillatory mode to behave as $0.9\nu(Re - Re_2)/D^2$; however, their results are with respect to the steady three-dimensional flow and not the base axisymmetric flow at $Re = 300$.

For all Reynolds numbers below $Re = 270$, the flow past a sphere reaches a steady-state solution. Moreover, when the flow is perturbed from that steady state, it returns back to that state after undergoing oscillations of decaying amplitude. The frequency associated with these oscillations is higher than the corresponding early linear frequency reported in table 3. A comparison of the two 'branches' of frequencies is given in figure 12 for $200 \leqslant Re \leqslant 300$, where the ranges of stability are also noted.

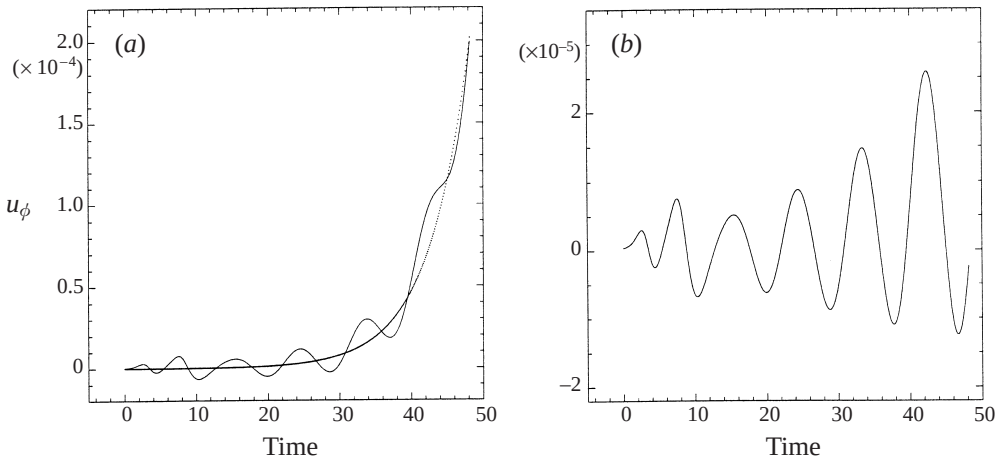

FIGURE 11. Time history of (*a*) the $m = 1$ mode of u_ϕ and (*b*) the oscillatory part of the $m = 1$ mode of u_ϕ at $(2.0D, 0.3D)$, $Re = 300$.

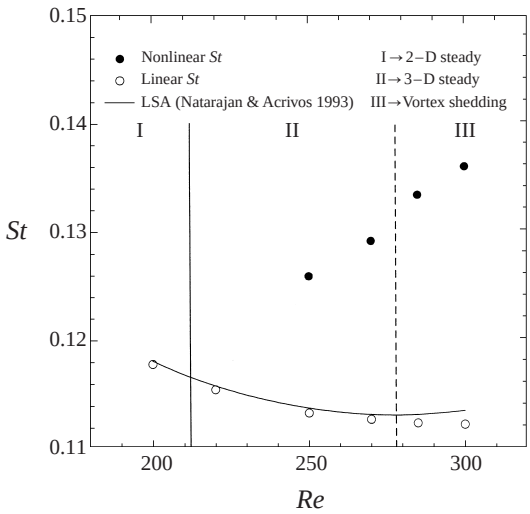

FIGURE 12. Strouhal number for linear and nonlinear oscillations vs. *Re*.

Frequencies are non-dimensionalized with the diameter of the sphere and the free-stream velocity ($St = fD/U_o$). The lower branch corresponds to the early stages of transition, with respect to the base axisymmetric flow, whereas the upper branch is the frequency with which the flow returns to steady state (up to $Re \leqslant 270$) after being perturbed from the three-dimensional steady-state solution. It is interesting to note that vortex shedding occurs only after the oscillatory 'linear' mode becomes unstable (between $270 \leqslant Re \leqslant 285$). Also, it seems that the shedding frequency at $Re = 285$ and $Re = 300$ does not depart in a dramatic way from the upper branch after the second transition to vortex shedding occurs. The characteristics of the flow after the transition to a vortex shedding state are given in the next section. The details of the flow during the low-amplitude oscillations without shedding were not investigated further, since the amplitude of these oscillations was below 10^{-5} and it was practically

impossible to extract and distinguish this oscillatory subdominant $m = 1$ mode from the non-oscillatory unstable $m = 1$ mode at the same Re.

For $220 \leqslant Re \leqslant 270$, the decay rates at which the flow returns to a time-independent state are smaller than the corresponding decay rates of the linear subdominant mode. This might be the reason for low-amplitude sustained oscillations without distinct vortex shedding, often reported in experiments below a Reynolds number of 270. It might be that incoming flow noise can trigger oscillations which seem to be self-sustained because of their very low decay rate. Such wave-like oscillations have been reported in the experiments of Möller (1938) for $Re \geqslant 200$, in the falling sphere experiments of Magarvey & Bishop (1965) for $270 \leqslant Re \leqslant 290$, and in the experiments of Sakamoto & Haniu (1990, 1995) for $Re < 300$.

5. Transition to unsteady flow

The flow past a sphere is known experimentally to result in a periodic (and eventually chaotic) wake as the Reynolds number increases. The second transition that leads to a time-dependent solution occurs between $Re = 270$ and $Re = 285$, according to our direct simulations. This value is considerably higher than the corresponding critical Reynolds number for the flow past a cylinder which is only 40. Direct numerical simulations were performed for Reynolds numbers 285, 300, 500, and 1000.

5.1. *Single-frequency vortex shedding: Re* = 285–300

The flow at $285 \leqslant Re \leqslant 300$ reaches a time-periodic final state with vortex shedding, and the Strouhal number associated with this shedding is plotted in figure 12. The basic wake structure, which consists of a succession of interconnected vortex loops, is similar to that observed in visualization experiments like those of Magarvey & Bishop (1961), Achenbach (1974) and Sakamoto & Haniu (1990). A plot of the drag coefficient for $Re = 300$ is given in figure 13(*a*); the drag coefficient increases from 0.6461 for the steady axisymmetric flow at the same Reynolds number up to an average value of 0.6714 after the vortex shedding process is fully developed. The power spectrum of the history of the drag coefficient is plotted in figure 13(*b*). The flow at $Re = 285$ and 300 maintains planar symmetry around the plane on which the shedding process is initiated, even though it has lost its axial symmetry. To demonstrate this, isosurfaces of constant streamwise vorticity are plotted in figure 14, which show that the vortex loops are always shed from the sphere with the same orientation. The dark and light colours denote positive and negative streamwise vorticity of the same magnitude, respectively. This figure may be compared with experimental and numerical results reported in Johnson & Patel (1999). In particular, flow visualization results shown in figure 39(*a*, *b*) of their paper are in very good agreement with figure 14.

Further downstream in the wake, the only frequency present is the non-dimensional shedding frequency (0.136 at $Re = 300$) and its superharmonics as shown in figures 15(*a*) and 15(*b*), where the time history of the azimuthal velocity component and its power spectrum are plotted for a point $5.75D$ downstream from the sphere.

Also, time histories of the three velocity components are plotted for two points in the near wake at $z = 1D, r = 0.2D$ and at azimuthal locations which differ by 67.5°. The streamwise component is plotted in figure 16(*a*), the radial component in figure 16(*b*), and the azimuthal component in figure 16(*c*). As can be observed from these figures, the amplitude of the waveform of the fluctuating velocities stays constant in

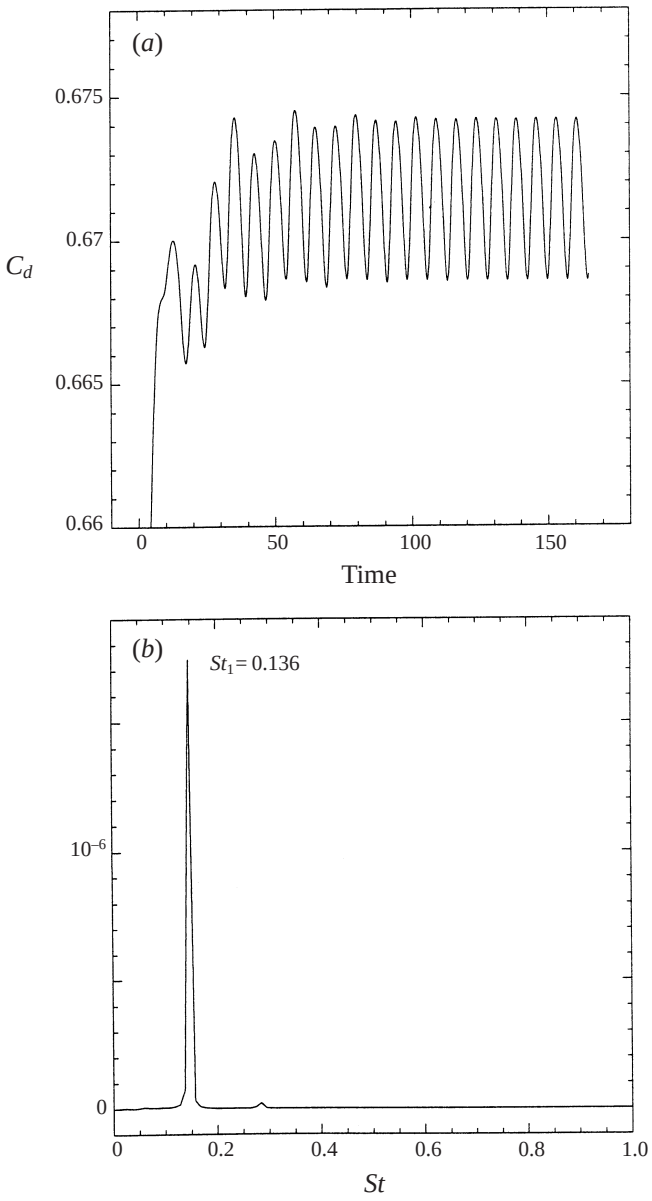

FIGURE 13. (*a*) Time history of the drag coefficient C_d and (*b*) its power spectrum, $Re = 300$.

time for the two points, suggesting that the hairpin vortices are always shed with the same orientation from the sphere.

Because of the planar symmetry observed in the shedding process, the time-averaged flow at Reynolds numbers 285 and 300 is three-dimensional and not axisymmetric. The streamwise velocity along the axis for the average flow is plotted in figure 17(*a*), whereas the same plot for the axial RMS velocity is given in figure 17(*b*). The end of the recirculation region along the axis, for the time-average flow, is at 1.3745 diameters downstream from the rear end of the sphere for $Re = 285$, and at 1.3478 diameters for $Re = 300$. A comparison of the computed average streamwise velocity

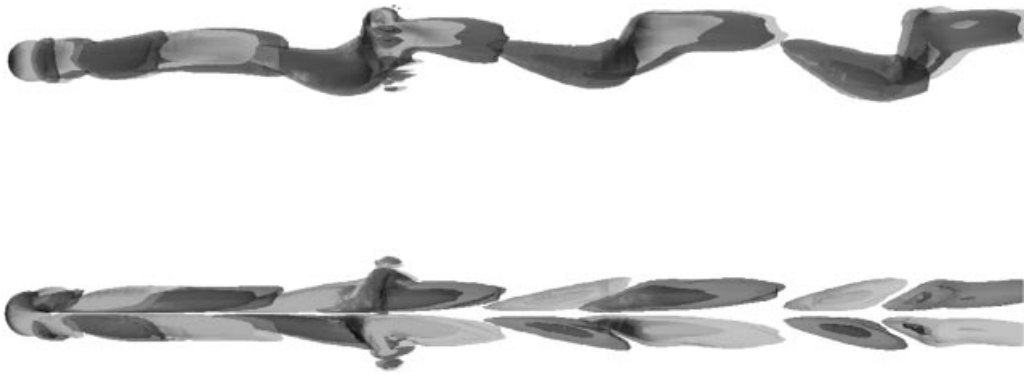

FIGURE 14. Isosurfaces of streamwise vorticity for flow past a sphere at $Re = 300$.

along the centreline for $Re = 285$ and 300 and the experimental results of Wu & Faeth (1993) for $Re = 280$ is also given in figure 17(*a*). From figure 17(*b*), it can be observed that there appears to be a global maximum of the RMS streamwise velocity very close to the end of the recirculation region for $Re = 300$ and a local maximum for the $Re = 285$ case. The points correspond to values reported by Wu & Faeth (1993) for $Re = 280$, which in their paper are normalized by the average streamwise velocity. As can be seen from the figure, there is reasonable agreement for all z except very close to the sphere, where the average streamwise velocity is very low. This leads to significant deviations in the near wake which are probably due to normalization. In addition, the shape of the RMS curve and the location of its maximum for $Re = 285$, at approximately 5 diameters downstream of the sphere, agree with results in Ormières *et al.* (1998) and Provansal & Ormières (1998), who report the energy of the fluctuation as function of z/D for this Re range.

It is of interest to note that Wu & Faeth (1993) reported both the first and the second bifurcation of flow past a sphere at approximately the same Re obtained by linear stability analysis (Natarajan & Acrivos 1993), and by the direct numerical simulations reported here. Ormières *et al.* (1998) on the other hand, who focused on the second transition, report an interesting observation in the discussion of figure 4 in their paper, which may imply the presence of a convectively unstable oscillatory mode before the appearance of the second absolute instability at approximately $Re = 280$. They report that when the flow is forced upstream with random noise, even for Re below the second transition, the fluctuation energy first grows downstream and then decays in a way very similar to the results plotted in figure 17(*b*). This may indicate the existence of a convectively unstable mode which becomes absolutely unstable after the second critical Re is reached; this, however, is a subject for further investigation.

5.2. *Higher Reynolds number vortex shedding: Re = 500–1000*

A numerical simulation was performed at $Re = 500$, starting from steady axisymmetric flow by imposing a small three-dimensional disturbance on the $m = 1$ azimuthal mode. The flow quickly becomes three-dimensional and results in vortex shedding (see figure 18). The wake structure is similar to the one observed at $Re = 300$, but as is evident from figure 18 the vortex loops are shed from the sphere with different orientation. The planar symmetry observed at $Re = 300$ is not preserved at $Re = 500$. This is also evident from figure 19(*a–c*) and in particular when compared with the equivalent figures for $Re = 300$ in figure 16(*a–c*). Points A and B are at the same z, r location but their azimuthal location differs by 90°. It can be observed that for $Re = 500$

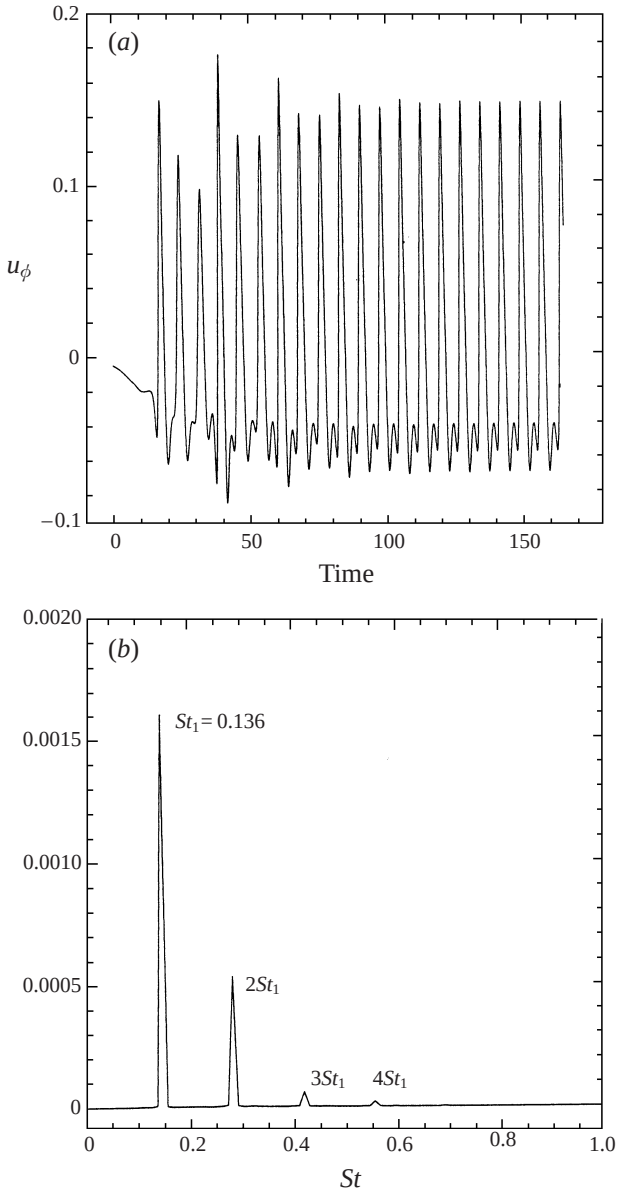

FIGURE 15. (*a*) Time history of u_ϕ and (*b*) its power spectrum at $z = 5.75D, r = 0.3D, Re = 300$.

the velocities at the two points oscillate around the same values, in contrast to what happens at $Re = 300$. This would imply that the time-average flow for $Re = 500$ is axisymmetric, in contrast to what is observed below $Re = 300$, where the average flow is three-dimensional; this phenomenon corresponds to an increase of symmetry in the average flow as Re increases.

This transition from a one-frequency flow to an almost chaotic system occurs between $Re = 300$ and 500 in our simulations, and is reported to occur at around $Re = 420$ by Sakamoto & Haniu (1990, 1995). There seems to be a lower incommensurate frequency associated with the loss of planar symmetry which is approximately equal

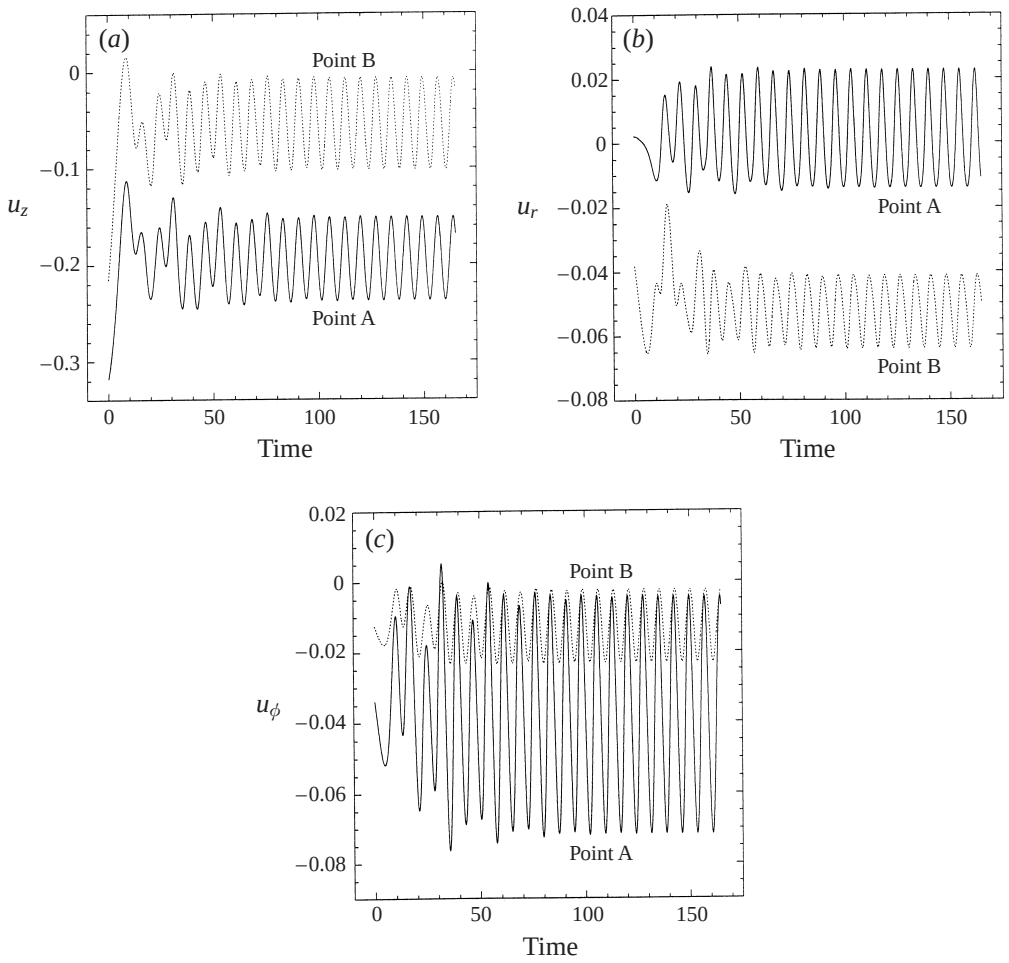

FIGURE 16. Time history of (*a*) u_z (*b*) u_z and (*c*) u_ϕ at $(1.0D, 0.2D)$, $Re = 300$.

to 0.045, and has to do with the irregular rotation of the separation point azimuthally around the rear part of the sphere, leading to the more complicated wake pattern observed in figure 18. Even though the vortex-loop wake structure at $Re = 500$ is quite distorted by the slow rotation of the separation point, the flow is still in an early transitional state and no small-scale structures are present.

The simulation at $Re = 500$ was carried out for a total of 200 time units, and only the last 120 units, which were in a statistically steady state, were used for evaluation of frequencies in power spectra. Time spectra at $Re = 500$ have pronounced peaks at the Strouhal number associated with the shedding, which is equal to 0.167 (the blocking factor was 1.2%). This frequency was dominant at all locations downstream from the sphere, and was obtained by averaging the values obtained at several history points in the near wake, which were not significantly different from each other. Figure 20(*a*) shows the time variation of the axial velocity component at $z = 2.0$, $r = 0.3$ and its power spectrum. There is a dominant peak at the Strouhal number 0.167. A power spectrum at another downstream point, $z = 2.5$, $r = 0$, plotted in figure 20(*b*), shows the existence of the lower frequency, approximately equal to 0.045, and the Strouhal frequency. Even though the lower frequency of the order of 0.045 is present in many

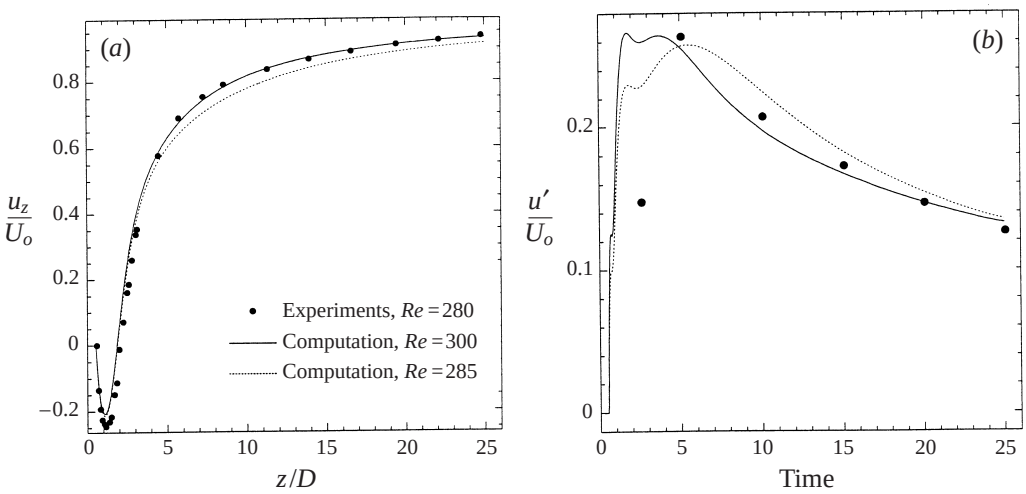

FIGURE 17. (*a*) Average streamwise velocity along the axis, for $Re = 285, 300$ compared with experimental results from Wu & Faeth (1993) for $Re = 280$. (*b*) RMS streamwise velocity along the axis, for $Re = 285, 300$.

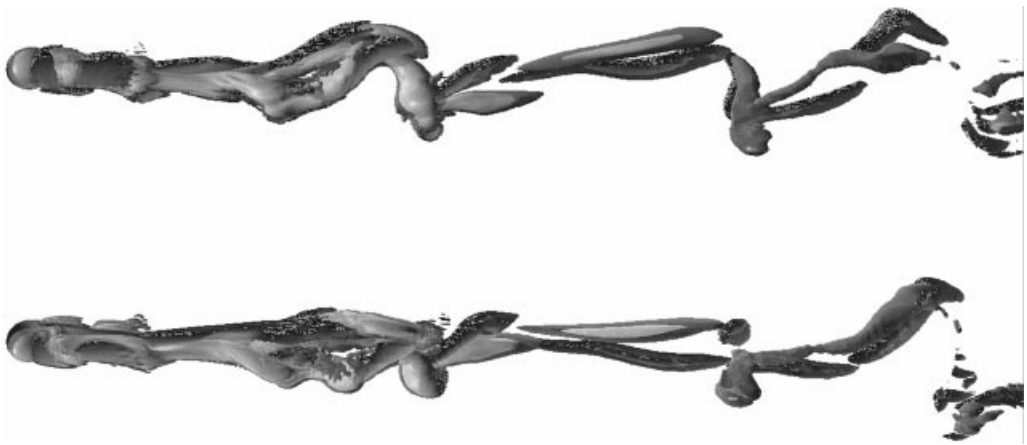

FIGURE 18. Isosurfaces of streamwise vorticity for flow past a sphere at $Re = 500$.

of the power spectra, longer time traces are needed for a more accurate evaluation of this frequency.

In his experiments, Achenbach (1974) reports two values for the Strouhal number at $Re = 500$, corresponding to two different spheres and blocking ratios; the first is about 0.163 and corresponds to a blockage of about 0.6% and the second is about 0.174 and corresponds to blockage of about 2.6%. His experiments were performed in a round pipe, in a similar way to our simulations. Kim & Durbin (1988) report a Strouhal number about 0.171 for $Re = 500$ and their blockage ratio is less than 0.01% for this Reynolds number; their experiments were performed in a wind tunnel of rectangular cross-section. Finally, Sakamoto & Haniu (1990) find a Strouhal number between 0.175 and 0.18 for $Re = 500$.

Experimentally, smaller scales appear and a more chaotic flow occurs when the Reynolds number exceeds 800. A direct simulation was performed at $Re = 1000$ using

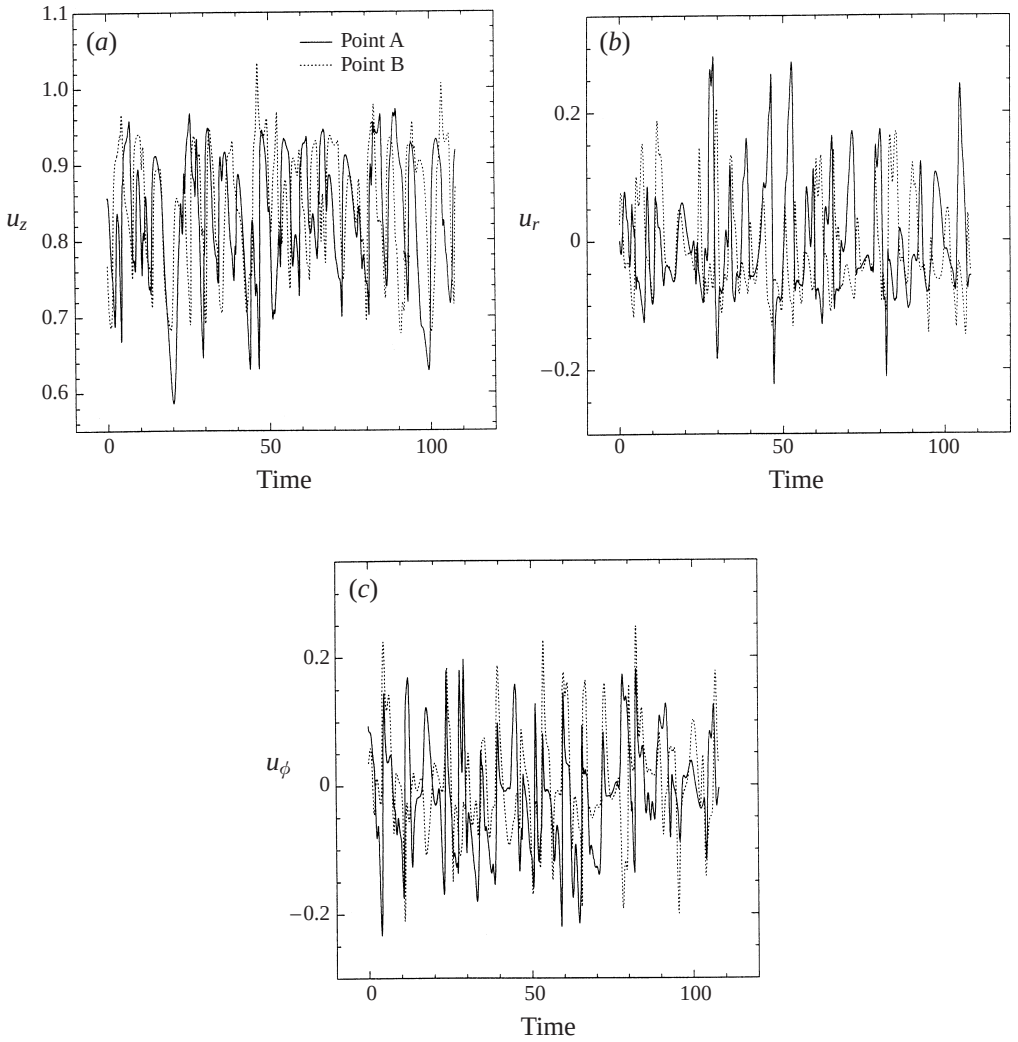

FIGURE 19. Time history of (*a*) u_z, (*b*) u_r and (*c*) u_ϕ at $(5.75D, 0.3D)$, $Re = 500$.

over 2.5×10^6 degrees of freedom. The results from this simulation reveal that small scales are indeed present in the flow field and their origin is a Kelvin–Helmholtz-like instability of the cylindrical shear layer that results from the separation of the boundary layer on the sphere. Visual evidence of the presence of roll-up of the shear layer and the appearance of small scales is shown in figure 21 in terms of isocontours of azimuthal vorticity, in particular in the lower half of the figure. The large-scale wake structure is similar to that at $Re = 500$; lower frequencies of the same order as at $Re = 500$ are observed, even though they have not been accurately determined as longer time traces are needed. The small scales associated with the shear-layer instability, cause a rapid distortion of the large vortex structures and eventually render the wake turbulent.

The simulation at $Re = 1000$ was advanced for a total of 270 time units, starting with initial conditions from the flow at $Re = 500$, and was time averaged for the last 130 time units, after it was verified that it had reached a statistically steady

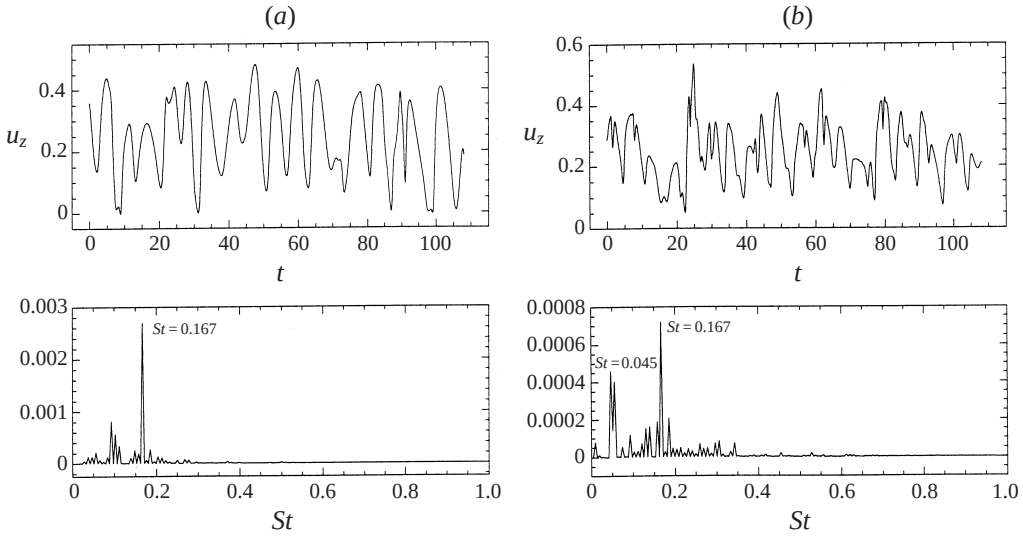

FIGURE 20. Time history and power spectrum of u_z at (*a*) $z = 2.0D, r = 0.3D$, and (*b*) $z = 2.5D, c = 0, Re = 500$.

FIGURE 21. Isocontours of azimuthal vorticity for flow past a sphere at $Re = 1000$.

state. At $Re = 1000$, the Strouhal number has increased to $St_1 = 0.195$ (see figure 22*a*). At points in the near wake of the sphere, where the roll-up of the shear layer appears to occur, a second higher frequency is observed at $St_2 \approx 0.35$ (these values have been determined, for all cases, by averaging the frequencies observed at several history points in the near wake), as can be seen in figure 22(*b*). Both values are in agreement with the Strouhal numbers reported in experiments. In the experiments of Kim & Durbin (1988), the lower frequency is found to be between 0.187 and 0.202 at $Re = 1000$; the higher frequency mode is measured to be between 0.33 and 0.37 (figure 2 in Kim & Durbin 1988). As mentioned in § 1, Achenbach (1974) regarded all the observed frequencies as being due to vortex shedding and only measured the higher frequency mode. His reported value of 0.39 is close to our measured value of 0.35 for this second mode. The values reported by Sakamoto & Haniu (1990, 1995), between 0.195 and 0.205, for the vortex shedding Strouhal number, and 0.29 and 0.34 for the second higher frequency mode are also in agreement with our results.

The flow at $Re = 1000$ was simulated until a statistically steady state was reached

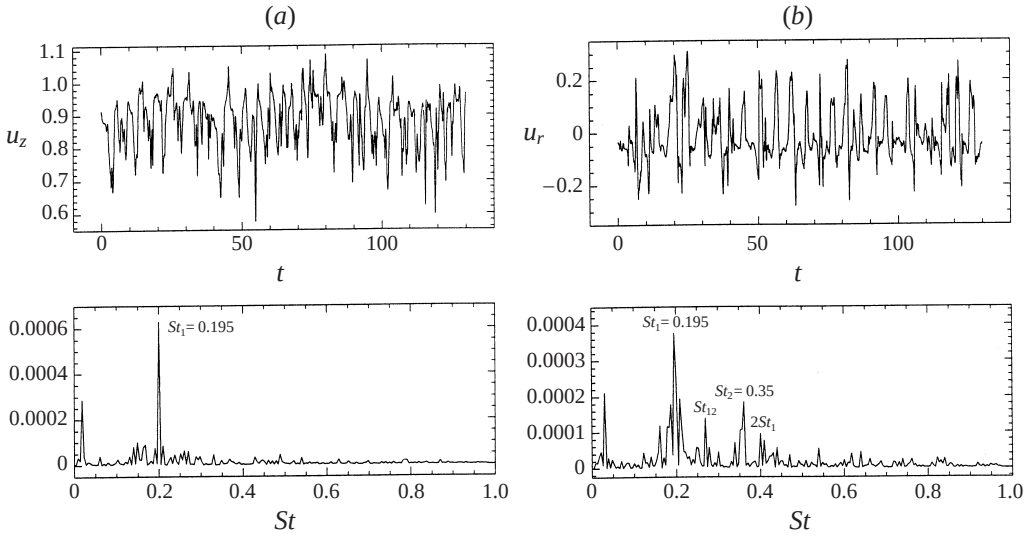

FIGURE 22. Power spectrum for time history of u_z at (*a*) $z = 2.5D, r = 0.3D$, (*b*) $z = 5.75D, c = 0.3D, Re = 1000$.

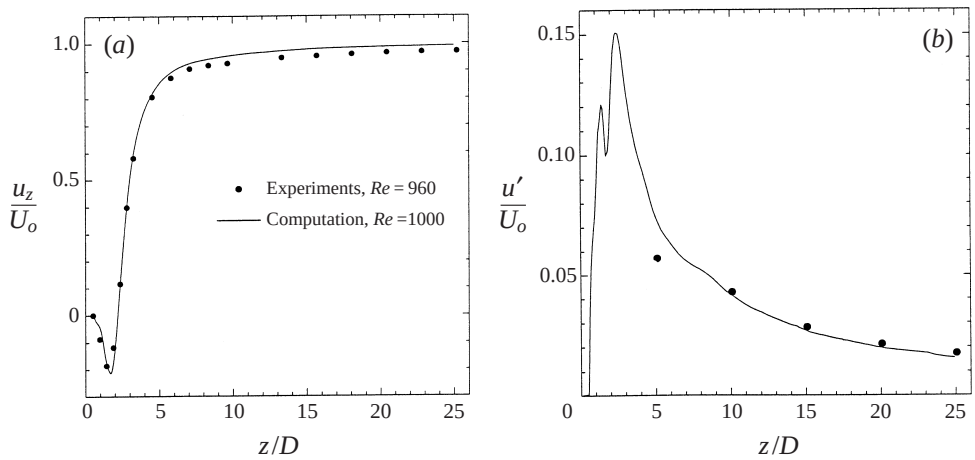

FIGURE 23. (*a*) Average and (*b*) RMS streamwise velocity along the axis for $Re = 1000$. Experimental data are from Wu & Faeth (1993).

and then was time averaged for 130 time units, which corresponds to about 30 shedding periods. A plot of the average streamwise velocity along the centreline is given in figure 23(*a*) together with the experimental data of Wu & Faeth (1993) for $Re = 960$. It can be seen that the length of the recirculation is approximately 1.7 diameters from the rear end of the sphere, which agrees well with the experimental results for $Re = 960$. The root mean square of the streamwise velocity along the axis is given in figure 23(*b*) together with measured values from Wu & Faeth (1993). Again, because of the normalization of the RMS velocities in the data of Wu & Faeth (1993) with the mean streamwise velocity, which is very low in the near wake, a small error in the local measured mean velocity results in a much larger error in the normalized RMS value; further downstream the agreement is improved. The computed maximum

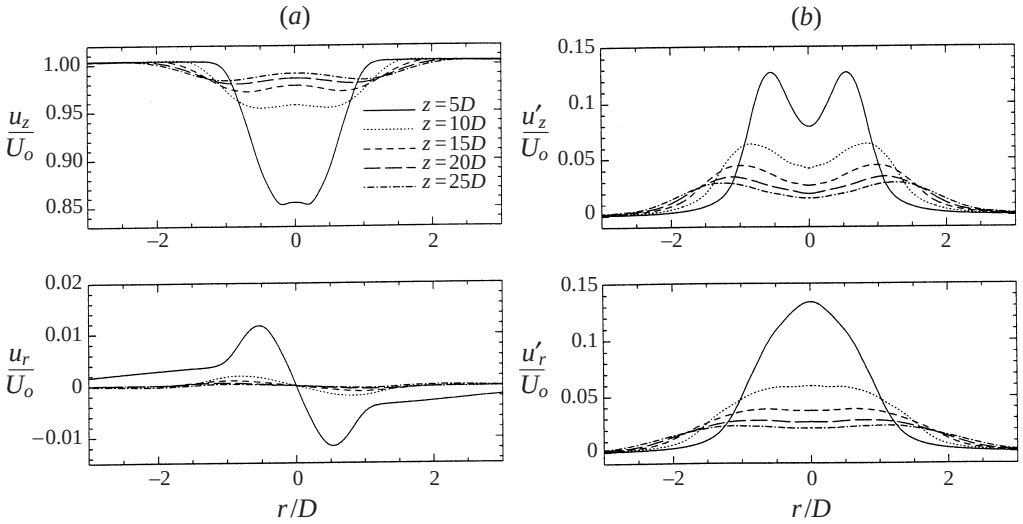

FIGURE 24. (*a*) Average and (*b*) RMS streamwise and radial velocities along the radial direction for different z locations for $Re = 1000$.

of the streamwise RMS velocity along the axis is found to be very close to the end of the recirculation region of the average flow. This was found to be the case for lower Re as well (i.e. $Re = 300$) and thus it seems that this phenomenon is rather independent of the Reynolds number.

The time-average location of the separation circle at $Re = 1000$ is found to be at 102° from the front end of the sphere. The separation circle at $Re = 300$ was found to be at 111°. Radial profiles of the streamwise and radial velocities of the time-average flow at $Re = 1000$ at different z downstream stations are plotted in figure 24(*a*). Radial profiles of the RMS values of the streamwise and radial velocity components for different streamwise locations are shown in figure 24(*b*).

In an attempt to examine the coherence of the shedding process in the azimuthal direction, histories of flow quantities at four points located at 2.7 diameters downstream of the sphere were traced in time. The points are at the same $z = 2.7$ and $r = 0.3$ location but their azimuthal location differs by 90°, i.e. $\phi_1 = 0°$, $\phi_2 = 90°$, $\phi_3 = 180°$, and $\phi_4 = 270°$. Auto- and cross-correlation functions were calculated from the time traces at points 1, 2, 3, and 4 as

$$\mathscr{R}_{ij}(\tau) = \lim_{T\to\infty} \frac{1}{T} \int_0^T u_i(t)\, u_j(t+\tau)\, \mathrm{d}t, \tag{5.1}$$

where the indices specify the point. The autocorrelation function is defined as

$$\mathscr{R}_{ii}(\tau) = \lim_{T\to\infty} \frac{1}{T} \int_0^T u_i(t)\, u_i(t+\tau)\, \mathrm{d}t, \tag{5.2}$$

where u_i and u_j are the instantaneous fluctuating values of time-traced quantities at points i and j, respectively. The product of the autocorrelation functions of signals u_i and u_j for $\tau = 0$ is used for the normalization of the cross-correlation coefficient $R_{ij}(\tau)$:

$$R_{ij}(\tau) = \frac{\mathscr{R}_{ij}(\tau)}{(\mathscr{R}_{ii}(0)\mathscr{R}_{jj}(0))^{1/2}}. \tag{5.3}$$

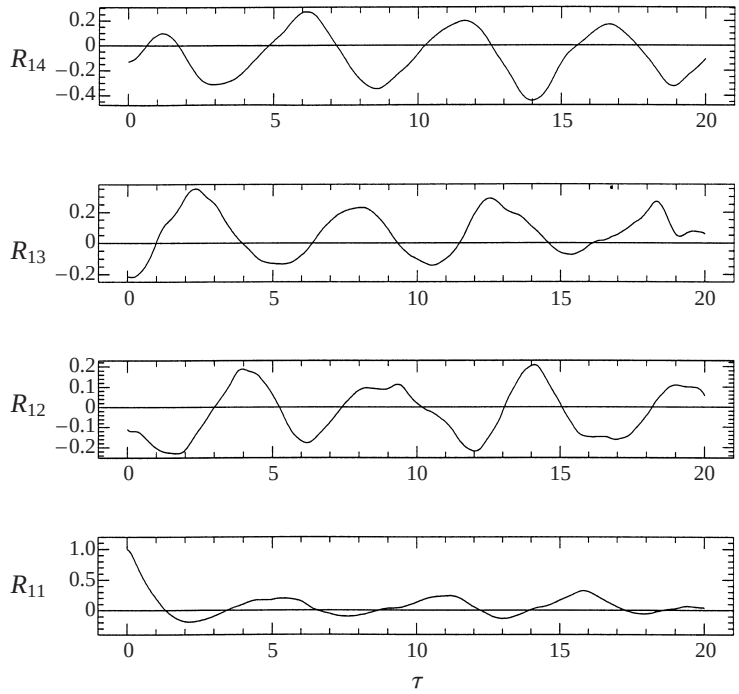

FIGURE 25. Autocorrelation coefficient $R_{11}(\tau)$, and cross-correlation coefficients $R_{12}(\tau)$, $R_{12}(\tau)$, and $R_{12}(\tau)$, at $Re = 1000$ (from bottom to top).

The auto- and cross-correlation coefficients are plotted for the streamwise velocity component, u_z, in figure 25 for the points 11, 12, 13, and 14, respectively from bottom to top. It can be observed that the phase angle between the time traces at the four points is approximately equal to the difference in their angular position in the azimuthal direction, as suggested by Achenbach (1974), possibly indicating some rotation mechanism in the azimuthal direction. However, more work is needed to understand this process.

6. Summary and concluding remarks

The viscous incompressible flow past a stationary sphere was investigated using numerical simulations. The focus of the investigation was to identify the transitions that the flow undergoes with increasing Reynolds number, as well as their underlying physical mechanisms. The range of Reynolds number investigated was from $Re = 25$ to 1000 using direct numerical simulation. A mixed spectral element/Fourier spectral method has been used, which is specifically designed for the study of three-dimensional flows in axisymmetric geometries. A special Jacobi-type polynomial is used on the axis of symmetry for the efficient treatment of the 'pole' problem, leading to an efficient and spectrally accurate way of removing geometrical singularities. This method has been verified and has been optimized for both serial and parallel computing environments.

This investigation started with the simulation of steady axisymmetric flow past a sphere in the low Reynolds number range. Flow parameters like wake length, separation angle and drag coefficient were calculated and were found in good agreement with other axisymmetric simulations and experimental results. According to the cur-

rent simulations, the first transition of this flow is a linear *regular* bifurcation and results in a three-dimensional steady-state flow field, similar to experimental results on falling spheres and linear stability analyses by Natarajan & Acrivos (1993). Numerical results from the early stages of this linear transition were compared with results from linear stability analysis in terms of growth rates and qualitative shape of the unstable eigenmodes; results from these two methods are found to be in very good agreement. More recent numerical simulation results (Johnson & Patel 1999) agree very well with our results for $Re \leqslant 300$.

Therefore, in contrast to the case of the flow past a cylinder, it is the second transition that leads to time dependence and vortex shedding for the flow past a sphere. The basic wake structure consists of a succession of interconnected vortex loops which, for low Reynolds numbers, are shed with the same orientation from the sphere; this results in planar symmetry which is observed in the flow up to a Reynolds number between 350 and 450. Simulations for $Re = 500$ reveal that this planar symmetry is lost and that vortices are shed with different chaotic orientation. At even higher Reynolds numbers, small scales appear in the flow, because of the Kelvin–Helmholtz instability of the cylindrical shear layer emanating from the sphere, and the wake is rendered turbulent. It is also found that, even at high Reynolds numbers where the wake is in a turbulent state, a large-scale wake structure is still evident. Wake structure, Strouhal number, drag coefficient and other quantitative characteristics of the flow are in good agreement with reported experimental work.

This work was partially supported by the ONR and DARPA. The authors would like to thank Professor Akiva Yaglom for comments and suggestions on, and interest in, this work.

REFERENCES

Achenbach, E. 1974 Vortex shedding from spheres. *J. Fluid Mech.* **62**, 209.

Batchelor, G. K. 1967 *An Introduction to Fluid Dynamics*. Cambridge University Press.

Fornberg, B. 1988 Steady viscous flow past a sphere at high Reynolds numbers. *J. Fluid Mech.* **190**, 471.

Gebing, H. 1994 Numerische Simulation und topologish-physikalishe Analyse der instationären, dreidimensionalen, abgelösten Wirbelströmungen an einer Kugel und an Rotationsellipsoiden. PhD thesis, Georg-August-Universität Göttingen.

Gottlieb, D. & Orszag, S. A. 1977 *Numerical Analysis of Spectral Methods: Theory and Applications*. SIAM, Philadelphia.

Gresho, P. M. & Sani, R. L. 1987 On pressure boundary conditions for the incompressible Navier–Stokes equations *Intl J. Numer. Meth. Fluids* **7**, 111.

Johnson, T. A. & Patel, V. C. 1999 Flow past a sphere up to a Reynolds number of 300 *J. Fluid. Mech.* **378**, 19.

Karniadakis, G. E., Israeli, M. & Orszag, S. A. 1991 High-order splitting methods for the incompressible Navier–Stokes equations. *J. Comput. Phys.* **97**, 414.

Kim, H. J. & Durbin, P. A. 1988 Observations of the frequencies in a sphere wake and of drag increase by acoustic excitation. *Phys. Fluids* **31**, 3260.

Kim, I. & Pearlstein, A. J. 1990 Stability of the flow past a sphere. *J. Fluid Mech.* **211**, 73.

Leonard, A. & Wray, A. 1982 A new numerical method for the simulation of 3-D flow in a pipe. In *8th Intl Conf. on Numerical Methods in Fluid Dynamics, Aachen, West Germany*, p. 335.

Maday, Y. & Patera, A. T. 1987 Spectral element methods for the Navier–Stokes equations. *State-of-the-Art Surveys in Computational Mechanics*. ASME.

Magarvey, R. H. & Bishop, R. L. 1961 Wakes in liquid–liquid systems. *Phys. Fluids* **4**, 800.

Magarvey, R. H. & Bishop, R. L. 1965 Vortices in sphere wakes. *Can. J. Phys.* **43**, 1649.

Möller, W. 1938 Experimentelle Untersuchungen zur Hydrodynamik der Kugel. *Phys. Z.* **39**, 57.

Nakamura, I. 1976 Steady wake behind a sphere. *Phys. Fluids* **19**, 5.

Natarajan, R. & Acrivos, A. 1993 The instability of the steady flow past spheres and disks. *J. Fluid Mech.* **254**, 323.

Ormières, D., Provansal, M. & Barrantes, A. 1998 Transient and forced regimes in the wake of a sphere. In *Advances in Turbulence VII* (ed. U. Frisc), pp. 81–84. Kluwer.

Orszag, S. A. 1974 Fourier series on spheres. *Mon. Weather Rev.* **102**, 56.

Patera, A. T. 1984 A spectral element method for fluid dynamics; Laminar flow in a channel expansion. *J. Comput. Phys.* **54**, 468.

Provansal, M. & Ormières, D. 1988 Étude expérimentale de I'instabilité du sillage d'une sphère. *C. R. Acad. Sci. Paris* **326** IIb, 489–494.

Sakamoto, H. & Haniu, H. 1990 A study on vortex shedding from spheres in a uniform flow. *Trans. ASME J. Fluids Enging* **112**, 386.

Sakamoto, H. & Haniu, H. 1995 The formation mechanism and shedding frequency of vortices from a sphere in uniform shear flow. *J. Fluid Mech.* **287**, 151.

Schlichting, H. 1979 *Boundary-Layer Theory*, 7th edn. McGraw-Hill.

Shirayama, S. 1992 Flow past a sphere: topological transitions of the vorticity field. *AIAA J.* **30**, 349.

Taneda, S. 1956 Experimental investigation of the wake behind a sphere at low Reynolds numbers. *J. Phys. Soc. Japan* **11**, 1104.

Tomboulides, A. G. 1993 Direct and large-eddy simulation of wake flows: flow past a sphere. PhD thesis, Princeton University.

Tomboulides, A. G., Israeli, M. & Karniadakis, G. E. 1989 Efficient removal of boundary-divergence errors in time-splitting methods. *J. Sci. Comput.* **4**, 291.

Wu, J. S. & Faeth, G. M. 1993 Sphere wakes in still surroundings at intermediate Reynolds numbers. *AIAA J.* **31**, 1448.